



Decreased Local Specialization of Brain Structural Networks Associated with Cognitive Dysfunction Revealed by Probabilistic Diffusion Tractography for Different Cerebral Small Vessel Disease Burdens

Mengmeng Feng¹ · Hongwei Wen² · Haotian Xin¹ · Shengpei Wang^{3,4} · Yian Gao⁵ · Chaofan Sui⁵ · Changhu Liang^{1,6} · Lingfei Guo⁶

Received: 31 May 2023 / Accepted: 14 August 2023 / Published online: 22 August 2023
© The Author(s) 2023, corrected publication 2023

Abstract

To reveal the network-level structural disruptions associated with cognitive dysfunctions in different cerebral small vessel disease (CSVD) burdens, we used probabilistic diffusion tractography and graph theory to investigate the brain network topology in 67 patients with a severe CSVD burden (CSVD-s), 133 patients with a mild CSVD burden (CSVD-m) and 89 healthy controls. We used one-way analysis of covariance to assess the altered topological measures between groups, and then evaluated their Pearson correlation with cognitive parameters. Both the CSVD and control groups showed efficient small-world organization in white matter (WM) networks. However, compared with CSVD-m patients and controls, CSVD-s patients exhibited significantly decreased local efficiency, with partially reorganized hub distributions. For regional topology, CSVD-s patients showed significantly decreased nodal efficiency in the bilateral anterior cingulate gyrus, caudate nucleus, right opercular inferior frontal gyrus (IFGoperc), supplementary motor area (SMA), insula and left orbital superior frontal gyrus and angular gyrus. Intriguingly, global/local efficiency and nodal efficiency of the bilateral caudate nucleus, right IFGoperc, SMA and left angular gyrus showed significant correlations with cognitive parameters in the CSVD-s group, while only the left pallidum showed significant correlations with cognitive metrics in the CSVD-m group. In conclusion, the decreased local specialization of brain structural networks in patients with different CSVD burdens provides novel insights into understanding the brain structural alterations in relation to CSVD severity. Cognitive correlations with brain structural network efficiency suggest their potential use as neuroimaging biomarkers to assess the severity of CSVD.

Keywords Cerebral small vessel disease burden · Diffusion tensor imaging · probabilistic tractography · Structural network · Graph theory

Mengmeng Feng and Hongwei Wen contributed equally to this work and shared the first authorship. Lingfei Guo and Changhu Liang contributed equally to this work and shared the corresponding author.

✉ Changhu Liang
tigerlch@163.com

✉ Lingfei Guo
glfsci@163.com

¹ Department of Radiology, Shandong Provincial Hospital, Shandong University, Jing-wu Road No. 324, Jinan, Shandong 250021, China

² Key Laboratory of Cognition and Personality (Ministry of Education), Faculty of Psychology, Southwest University, Chongqing 400715, China

³ Research Center for Brain-inspired Intelligence, Institute of Automation, Chinese Academy of Sciences, ZhongGuanCun East Rd. 95 #, Beijing 100190, China

⁴ University of Chinese Academy of Sciences, Beijing, China

⁵ Department of Radiology, Shandong Provincial Hospital Affiliated to Shandong First Medical university, Jing-wu Road No. 324, Jinan, Shandong 250021, China

⁶ Key Laboratory of Endocrine Glucose & Lipids Metabolism and Brain Aging, Department of Radiology, Ministry of Education, Shandong Provincial Hospital Affiliated to Shandong First Medical University, Jinan, Shandong 250021, China

Introduction

Cerebral small vessel disease (CSVD), one of the most common diseases in older adults, plays a vital role in dementia and stroke [1, 2]. The clinical manifestations of CSVD mainly include cognitive decline, gait disturbance, and psychiatric disorders. It can be visualized on neuroimaging scans as lacune, white matter hyperintensity (WMH), perivascular space (PVS), cerebral microbleed (CMB), recent small subcortical infarct, cortical superficial siderosis, brain atrophy, cortical cerebral microinfarct and summary small vessel disease score on brain MRI scans [3]. Previous studies have focused on the effect of a single CSVD feature and thus may have overlooked other features, but these neuroimaging features often occur simultaneously. Therefore, Pim Klarenbeek et al. proposed the concept of total CSVD burden, which integrates four previously mentioned CSVD features, to comprehensively evaluate the cumulative effects of various CSVD features on the brain and more completely estimate the severity of CSVD [4].

Recently, some studies have begun to pay attention to the CSVD burden. The MRI-based CSVD burden score improved diagnostic accuracy for predicting new onset of dementia after intracerebral hemorrhage [5]. Previous studies have shown that the CSVD burden was associated not only with the degree of damage to fiber tracts and reduced cortical thickness in a wide range of brain regions but also with gait/balance function and cognitive impairment [6–8]. Chen et al. paid attention to the multi-dimensional effects of CSVD burden on Parkinson's disease (PD) and grouped PD patients according to the CSVD burden score (CSVD burden score 0–1 vs. 2–4). The results showed that motor dysfunction, cognitive impairment, depression, and anxiety were significantly worse in patients with severe CSVD than in those with mild CSVD [9]. A study on type 2 diabetes, divided patients into mild burden (0–1 points) group and moderate to severe burden (2–4 points) group based on the total CSVD burden score, demonstrated that the moderate to severe burden group was more likely than the mild burden group to have narrowed retinal arterioles, widened retinal venules, and lower arteriole-to-venule ratio [10]. These findings suggested that the CSVD burden affected the basic structure of gray and white matter in the brain, as well as the development and clinical manifestations of various diseases.

Despite these advances in research, the mechanism by which patients with different CSVD burdens exhibit clinical differences is still unclear. The relationship among different brain white matter structures should be taken seriously. The interregional interactions between anatomically separated structures could play important roles in processing complex clinical symptoms. Some studies on brain connectivity have

suggested that human whole-brain structural networks can be reconstructed using diffusion tensor imaging (DTI) and probabilistic tractography [11, 12]. Graph theory, a powerful approach to characterize the interregional connective features within networks [13], can be used to obtain many important topological properties of brain structural networks, such as small-world topology, highly connected hubs and modularity [14], which exactly addresses the problem of interactions between different brain structures being neglected in some studies. Moreover, graph theory analysis can detect subtle changes in WM structure networks that may be overlooked by traditional techniques when the disease is not too serious [15], so as to better reveal the separation and integration status of the networks and the transmission of information.

Graph theory analysis has become increasingly popular in studying the CSVD burden and brain networks in CSVD patients. Previous studies have noted that an increasing burden of CSVD was associated with decreased nodal efficiency [6, 16] and small-worldness, reduced integration (increasing path length and lower global efficiency) and increased segregation (increasing clustering coefficient) of brain structural networks [6, 17]. Rutger Heinen et al. reconstructed structural brain networks using fiber tractography followed by graph theoretical analysis, assessed the relationship between total CSVD burden score, global network efficiency and cognition and showed that for every one-point increase in the CSVD burden score, global network efficiency decreased by 0.260 SD units [18]. These results provide new insights into the impact of CSVD burden on the structural network disruptions.

Building on previous works showing impaired structural connectivity networks in CSVD patients and the correlation between the CSVD burden and network parameters, we investigated the differences in the topological organization of the WM structural networks in patients with different CSVD burdens and controls through probabilistic diffusion tractography and graph theory analysis. Since CSVD patients often tend to experience cognitive decline which is affected by CSVD burden, the purpose of this study was to determine the relationship between the graph theoretical quantitative metrics and cognitive parameters of different CSVD burden groups.

Materials and Methods

Subjects

This was a cross-sectional study approved by the institutional review board of Shandong Provincial Hospital Affiliated to Shandong First Medical University. Between

December 2018 and July 2022, 200 CSVD patients and 89 age-, sex- and education-matched healthy subjects were recruited in our study. Each participant voluntarily signed an informed consent form prior to the start of the study.

The inclusion criteria for CSVD patients comprised: (1) 40–75 years; (2) presence of lacune, WMH, PVS, CMB, recent small subcortical infarct, cortical superficial siderosis, brain atrophy, cortical cerebral microinfarct or summary small vessel disease score based on current MRI consensus standards [3].

The exclusion criteria included: (1) a history of stroke, brain trauma, epilepsy, brain tumors, intracerebral hemorrhage; (2) a history of major neurologic or psychiatric illnesses; (3) a history of alcohol or substance abuse; (4) a history of thrombolysis; (5) Alzheimer's disease, Parkinson's disease and other related diseases that cause cognitive impairment; (6) acute complications of type 2 diabetes and severe hypertension; (7) with significant hearing, vision and speech impairment; (8) unable to tolerate MRI or claustrophobia.

MRI Acquisition and Evaluation

All subjects were imaged on a MAGNETOM Skyra 3.0 T MR scanner (Siemens Healthcare, Erlangen, Germany) using a product 32-channel head coil for signal reception. Diffusion weighted images (DWI) were acquired using a simultaneous multislice (SMS) accelerated single-shot echo planar imaging (EPI) sequence with the following parameters: repetition time (TR)=3000 ms, echo time (TE)=110 ms, 30 diffusion directions with $b=1700$ s/mm² and a single $b=0$ s/mm² acquisition, field of view (FOV)=220×220 mm, matrix size=110×110, 60 slices, and slice thickness=2.2 mm with no intersection gap. 3D T1-weighted images were acquired using a magnetization-prepared rapid gradient echo (MPRAGE) sequence with the following parameters: TR / TE=7.3 / 2.4 ms, inversion time (TI)=900 ms, flip angle=9°, FOV=240×240 mm, matrix size=256×256, 192 slices, and slice thickness=0.9 mm with no gap. In addition, T2-weighted imaging, fluid-attenuated inversion recovery (FLAIR) imaging, and susceptibility-weighted imaging (SWI) were acquired to detect brain abnormalities. All participants were required to be awake and quietly breathing until the end of the scan.

Two experienced radiologists blinded to the clinical data independently evaluated CSVD imaging features on all MRI images based on the STRIVE criteria (STAndards for ReportIng Vascular changes on Euroimaging) [3]. The CSVD burden is a pragmatic ordinal scale of 0–4 based on four MRI features of CSVD [4], their imaging performances and rating standards are included in the Supplementary materials. One point was awarded if ≥ 1 lacunes were

present; one point was awarded if periventricular WMH reaches grade 3 or deep WMH reaches grade 2 or 3; one point was awarded if there were moderate to severe (grade 2–3) PVS in the basal ganglia; and one point was awarded if ≥ 1 CMB were present. In this study, CSVD patients were further grouped into those with a mild CSVD burden (CSVD-m; burden score 0–1; 133; age: 62.11 ± 6.88 years) and those with a severe CSVD burden (CSVD-s, burden score 2–4; 67; age: 64.16 ± 5.48 years). This stratification was consistent with the previous studies [9, 10].

Cognitive Assessments

All participants underwent the Montreal Cognitive Assessment (MoCA) Beijing version (www.mocatest.org) which is a one-page 30-point test administered in 10 min [19]. The optimal cutoffs for detecting cognitive impairment was 13/14 points for illiterate individuals, 19/20 for individuals with 1–6 years of education, and 24/25 for individuals with 7 or more years of education [20]. In addition, a variety of executive functions, including flexibility, working memory and inhibition, were assessed. These tests included the following: the Rey auditory verbal learning test (AVLT) for assessing verbal memory abilities [21]; the symbol digit modalities test (SDMT) for evaluating attention and information processing speed [22]; the trail-making test (TMT) for evaluating attention, information processing speed, visual search and motor coordination [23]; and the Stroop color-word test (SCWT) [24]. The test implementer was professionally trained and qualified and had no knowledge of the subject grouping.

Image Preprocessing

Following data acquisition, all the 3D T1-weighted images were manually reoriented to their respective anterior commissure–posterior commissure (AC-PC) plane using the statistical parametric mapping (SPM8, <http://www.fil.ion.ucl.ac.uk/spm>) toolbox. Then, we used the FMRIB software library (FSL v5.09, <http://www.fmrib.ox.ac.uk/fsl>) for diffusion image processing. Briefly, brain masks were created from the b_0 image to remove nonbrain tissues using the Brain Extraction Tool (BET) in FSL. Second, eddy current distortions and motion artifacts were corrected by applying an affine alignment of each diffusion-weighted image to the b_0 image and adjusting the gradient orientations to adapt to the slight rotations because of head movement parameters. Finally, the diffusion tensor model was fitted to each voxel using FMRIB's diffusion toolbox (FDT v3.0), and the probabilistic distribution of fiber orientations from each voxel was estimated with a two-tensor model [25].

Network Construction

Network construction requires the following basic elements: nodes and connection edges, and the main steps are described in the following sections (detailed in Fig. 1).

Node definition: We defined the network nodes as in our previous study [12]. Briefly, individual T1-weighted images were coregistered to the b_0 images in the DTI space by using an affine transformation (FLIRT tool in FSL). The registered T1 images were then nonlinearly transformed to the ICBM152 T1 template in MNI space by using FNIRT tool in FSL. The inverse transformations were used to warp the automated anatomical labeling (AAL) atlas [26] from MNI space to each native DTI space. Of note, the nearest-neighbor interpolation method was used to preserve discrete labeling values. Using this procedure, we obtained 90 cortical and subcortical regions (45 for each hemisphere), each representing a node in the network (Supplementary Table 1).

Connection definition: To define the connections between brain regions, we performed probabilistic tractography. First, we used the *bedpostx* tool in FSL to run Markov Chain Monte Carlo sampling to estimate distributions on diffusion parameters at each voxel, which allows us to model crossing fibers within each voxel of the brain. Second, we used the *probtrackx* tool in FSL to perform probabilistic tracking. Briefly, we repetitively performed 5000 samplings

from the distributions of voxel-wise principal diffusion directions, each time computing a streamline through these local samples to generate a probabilistic streamline fiber. For a seed region, $5000 \times n$ streamline fibers were sampled; n is the number of voxels in the seed region. The number of streamline fibers passing through a given region divided by $5000 \times n$ was calculated as the connectivity probability from the seed region to the given region. The connection edges were defined as the above connectivity probability P_{ij} between regions i and j . In this study, each brain region based on the AAL atlas was selected as the seed region, and its connectivity probability to each of the other 89 regions was calculated. Thus, for each subject, a 90×90 probability weighted matrix was created to represent the constructed network. To remove spurious connections, the weakest connections under a given sparse threshold in the probability weighted matrix were discarded for each subject. To exclude the bias of a single sparse threshold, sparsity ranging from 6 to 24% with an interval of 1% was used as in previous studies [12, 27], and the network metrics were calculated at each threshold.

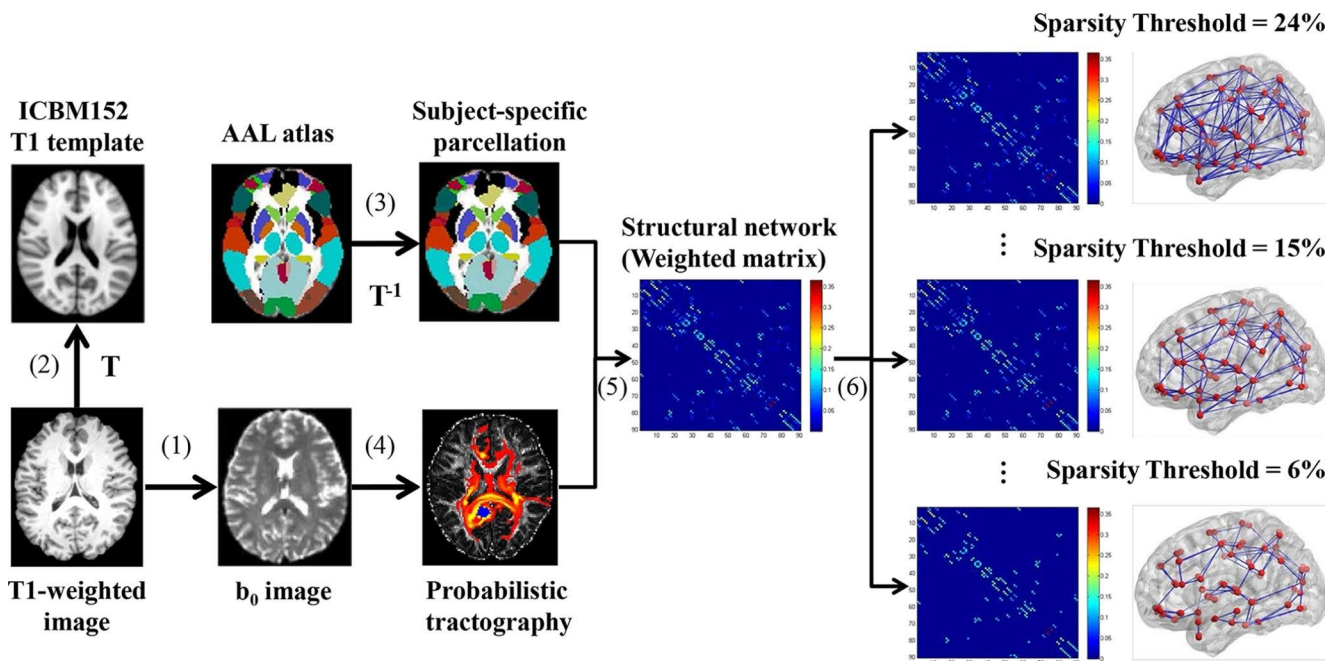


Fig. 1 Flowchart of white matter structural network construction (1) Register the T1-weighted image to the b_0 image in native DTI space for each subject by using an affine transformation. (2) The registered T1 images were then nonlinearly transformed to the ICBM152 T1 template in the MNI space, resulting in a nonlinear transformation (T). (3) Apply the inverse transformation (T^{-1}) to the AAL atlas (90 regions) in the MNI space, resulting in a subject-specific parcellation

of node regions in native DTI space. (4) For each region, estimate the connectivity probability with other brain regions by using probabilistic diffusion tractography. (5) Construct the 90×90 weighted network for each subject by computing the connection probability between each pair of regions. (6) Threshold the individual matrix using a sparsity ranging from 6 to 24% with an interval of 1%. The visualization of the sparse networks is represented in lateral view

Network Topological Analysis

To characterize the topological organization of WM structural networks, graph theoretical quantitative metrics were assessed at each threshold. The global properties include:

(1) The clustering coefficient (C_p) of the network, which is the average nodal clustering coefficient (C_i) over all nodes, and is computed as follows:

$$C_i = \frac{2}{k_i(k_i-1)} \sum_{j,k} \left(\bar{w}_{ij} \bar{w}_{jk} \bar{w}_{ki} \right)^{1/3}$$

where k_i is the degree of node i , and \bar{w} is the weight, which is scaled by the mean of all weights to control each subject's cost at the same level.

(2) The shortest path length (L_p) of network G , and is computed as follows:

$$L_p(G) = \frac{1}{N(N-1)} \sum_{i \neq j \in G} L_{ij}$$

where L_{ij} is defined as the length of the path for node i and node j with the shortest length. For weighted networks, the length of each edge was assigned by computing the reciprocal of the edge weight ($1/w_{ij}$).

(3–4) The normalized shortest path length $\lambda = L_p^{\text{real}}/L_p^{\text{rand}}$, and the normalized clustering coefficient $\gamma = C_p^{\text{real}}/C_p^{\text{rand}}$, in which L_p^{rand} and C_p^{rand} are the mean shortest path length and mean clustering coefficient of 100 matched random networks.

(5) The small-world index $\sigma = \lambda/\gamma$, and a real network would be considered to indicate a small world if $\gamma > 1$ and $\lambda \approx 1$.

(6) The global efficiency (E_{glob}) of network G measures the global efficiency of the parallel information transfer in network [28], which is computed as follows:

$$E_{\text{glob}}(G) = \frac{1}{N(N-1)} \sum_{i \neq j \in G} \frac{1}{L_{ij}}$$

(7) The local efficiency (E_{loc}) of network G reveals how much the network is fault tolerant and measures how efficient the communication is among the first neighbors of node i when it is removed, and is computed as follows:

$$E_{\text{loc}}(G) = \frac{1}{N} \sum_{i \in G} E_{\text{glob}}(G_i)$$

where G_i denotes the subgraph composed of the nearest neighbors of node i .

(8) The nodal efficiency (E_{nodal}), which measures the average shortest path length between a given node i and

all of the other nodes in the network and is computed as follows:

$$E_{\text{nodal}}(i) = \frac{1}{N-1} \sum_{i \neq j \in G} \frac{1}{L_{ij}}$$

Similar to previous studies, node i was considered a brain hub if $E_{\text{nodal}}(i)$ was at least one standard deviation (SD) greater than the average nodal efficiency of the network (i.e., $E_{\text{nodal}}(i) > \text{mean} + \text{SD}$). We also calculated the area under the curve (AUC) for each network metric (global and local topological properties) to provide a summarized scalar independent of single threshold selection. The regional network measure and hub analyses were all conducted on the AUC value of E_{nodal} . The graph theory analysis was implemented using a graph theoretical network analysis toolbox (GRETNA, <http://www.nitrc.org/projects/gretna/>) [29].

Between-Group Statistical Comparison and Correlation Analysis

One-way analysis of variance (ANOVA) and least significant difference (LSD) post hoc multiple comparisons were used to assess demographic parameters and cognitive test scores among the three groups, and the chi-square test was used to analyze the sex proportions. For global and nodal network metrics, one-way analysis of covariance (ANCOVA) was performed to investigate differences among the three groups, controlling age, sex and education level as covariates, with LSD post hoc tests for pairwise comparisons. Once significant intergroup differences were identified in any nodal topological metrics, we further assessed the Pearson's correlations between the nodal metrics and cognitive parameters for all groups using SPSS Version 24.0 (SPSS Inc, Chicago, IL, USA), and the significance level was set to $p < 0.05$ for all analyses.

Results

Demographic and Clinical Characteristics of the Subjects

The demographic and clinical characteristics of each group are summarized in Table 1. The CSVD-s group had significantly lower MoCA, the Rey auditory verbal learning test (AVLT), and the symbol digit modalities test (SDMT) scores and significantly higher the Stroop color-word test (SCWT) and the trail-making test (TMT) scores than the CSVD-m and control groups. In addition, the CSVD-m group had significantly lower SDMT scores than the control

Table 1 Demographic and clinical characteristics of CSVD patients and controls

| Characteristic | CSVD-s | CSVD-m | HC | P value (ANOVA / χ^2) | P value (post-hoc) | | |
|-------------------|----------------|-----------------|----------------|-----------------------------------|--------------------|----------------------|----------------------|
| | | | | | CSVD-s vs. HC | CSVD-s vs. CSVD-m | CSVD- m vs. HC |
| Sex | 43 M / 24 F | 70 M / 63 F | 40 M / 49 F | 0.058 ² | - | - | - |
| Age (y) | 64.16 ± 5.48 | 62.11 ± 6.88 | 61.43 ± 9.54 | 0.071 ^a | - | - | - |
| Hypertension | 54 (80.6%) | 67 (50.4%) | 32 (36.0%) | < 0.001 ² | - | - | - |
| Diabetes mellitus | 32 (47.7%) | 67 (50.4%) | 32 (36.0%) | 0.096 ² | - | - | - |
| Hyperlipidemia | 37 (55.2%) | 59 (44.4%) | 41 (46.1%) | 0.333 ² | - | - | - |
| Smoking | 17 (25.4%) | 36 (27.1%) | 15 (16.9%) | 0.196 ² | - | - | - |
| Education (y) | 11.13 ± 3.15 | 12.10 ± 3.29 | 12.38 ± 3.88 | 0.070 ^a | - | - | - |
| MoCA | 24.03 ± 2.97 | 25.26 ± 3.58 | 26.04 ± 3.79 | 0.003 ^a | 0.001 | 0.021 | 0.114 |
| AVLT | 54.76 ± 12.82 | 60.16 ± 13.14 | 63.11 ± 12.44 | < 0.001 ^a | < 0.001 | 0.006 | 0.100 |
| SDMT | 26.39 ± 11.24 | 31.55 ± 12.53 | 39.32 ± 14.05 | < 0.001 ^a | < 0.001 | 0.008 | < 0.001 |
| SCWT | 175.44 ± 55.79 | 147.36 ± 43.95 | 137.12 ± 50.35 | < 0.001 ^a | < 0.001 | < 0.001 | 0.133 |
| TMT (B-A) | 172.86 ± 94.78 | 127.47 ± 100.03 | 111.37 ± 93.14 | < 0.001 ^a | < 0.001 | 0.002 | 0.233 |
| WMHs (1 point) | 49 (73.1%) | 6 (4.5%) | - | < 0.001 ² | - | - | - |
| EPVs (1 point) | 59 (88.1%) | 40 (30.1%) | - | < 0.001 ² | - | - | - |
| CMBs (1 point) | 44 (65.7%) | 19 (14.3%) | - | < 0.001 ² | - | - | - |
| Lacunae (1 point) | 30 (44.8%) | 3 (2.3%) | - | < 0.001 ² | - | - | - |

Abbreviations: CSVD=cerebral small vessel disease; MoCA=Montreal Cognitive Assessment; AVLT=sum of Rey auditory verbal learning test (N1-7); SDMT=symbol digit modalities test; SCWT=sum of Stroop color-word test (stroop1-3); TMT=the trail-making test; TMT (B-A)=the difference between TMT-B and TMT-A; WMHs=white matter hyperintensities; EPVs=enlarged perivascular spaces; CMBs=cerebral microbleeds; CSVD-s=severe CSVD burden (score ≥ 2) group; CSVD-m=mild CSVD burden (score ≤ 1) group; HC=healthy controls; ²=chi-square test; ^a=ANCOVA test. The last four rows are the number of subjects who scored one point for each CSVD burden features in the two CSVD subgroups

group. No significant differences were found in age, sex or education among the three groups.

Altered Global Properties of WM Networks in CSVD-s Patients

Over the whole sparsity range, the CSVD-s, CSVD-m and control groups all exhibited high-efficiency small-world topology characterized by $\gamma > 1$, $\lambda \approx 1$ and $\sigma = \gamma / \lambda > 1$ (Fig. 2). Statistical comparisons (ANCOVA with LSD post hoc test) were performed to detect significant differences in global properties among the three groups. Compared with the CSVD-m and control groups, the CSVD-s group showed significantly ($p < 0.05$) decreased E_{loc} over a wide range of sparsity thresholds (Fig. 2b). No significant difference was found between the CSVD-m and control groups. Moreover, the CSVD-s group showed significantly decreased AUC values of E_{loc} compared with other groups (Table 2), indicating the consistency and robustness of significant alterations over sparsity thresholds. There was no significant difference in other global properties among groups.

Partially Reorganized Hub Distributions of WM Networks in CSVD-s Patients

For each group, the nodes were considered brain hubs if their E_{nodal} was at least one SD greater than the average E_{nodal} of the network [12, 27]. We found partially reorganized hub distributions among groups with eleven common hub regions, including the bilateral inferior occipital gyrus (IOG), opercular inferior frontal gyrus (IFGoperc), Heschl gyrus, right inferior parietal gyrus, angular gyrus, amygdala and left supramarginal gyrus (SMG) and posterior cingulate gyrus. The CSVD-s and control groups each had an additional hub region in the left hippocampus and angular gyrus, respectively, and the CSVD-m group lacked the left Rolandic operculum as a hub region (Table 3; Fig. 3a).

Altered Regional Properties of WM Networks in CSVD-s Patients

Ten brain regions exhibiting significantly (ANCOVA, $p < 0.05$) altered E_{nodal} among the three groups were identified (Table 4). Furthermore, using the LSD post hoc test, pairwise intergroup differences were also identified. Compared with the CSVD-m or control groups, the CSVD-s group exhibited significantly decreased E_{nodal} in the bilateral anterior cingulate gyrus (ACG), caudate nucleus, right

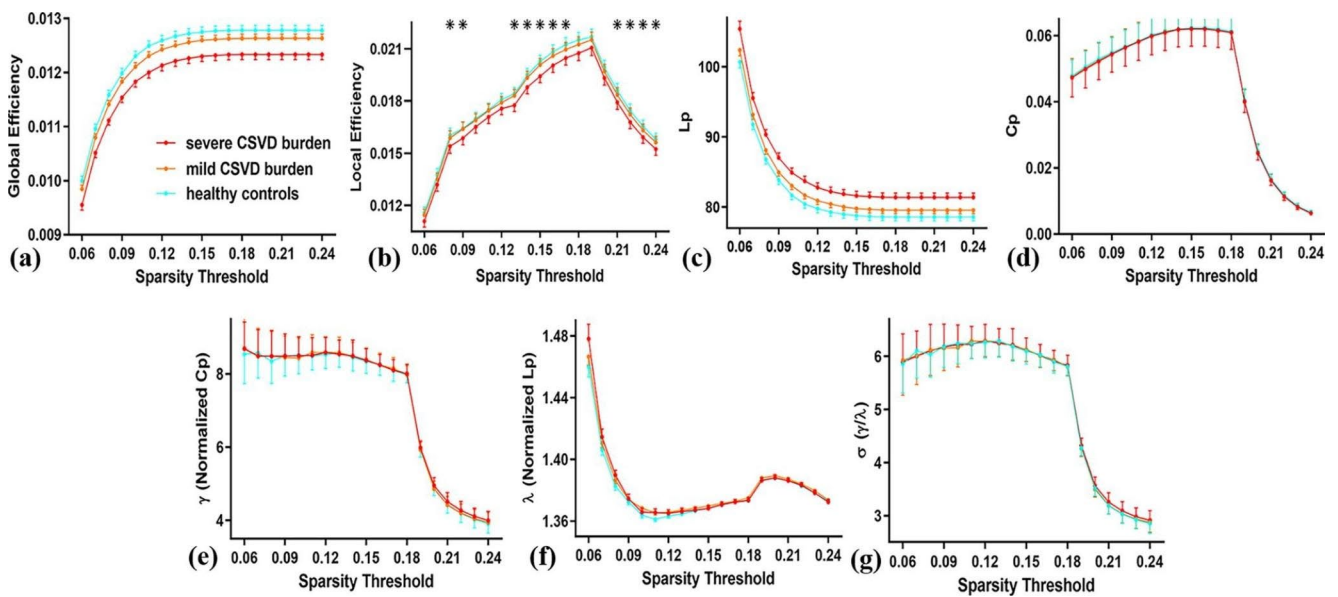


Fig. 2 Group comparisons of global topological properties. Data points marked with a star indicate the global property showing significant differences ($p < 0.05$, ANCOVA with LSD post-hoc test) in

the CSVD-s group compared with the CSVD-m and control groups under a corresponding sparsity threshold. There was no difference between the CSVD-m and control groups

Table 2 Group comparisons of AUC values of global properties

| Global property (AUC value) | CSVD-s | CSVD-m | HC | P value (ANCOVA) | P value (post-hoc) | | |
|-----------------------------|------------------|------------------|------------------|--------------------|--------------------|-------------------|---------------|
| | | | | | CSVD-s vs. HC | CSVD-s vs. CSVD-m | CSVD-m vs. HC |
| $E_{glob} (x^{e-2})$ | 1.19 ± 0.08 | 1.22 ± 0.09 | 1.24 ± 0.09 | 0.091 ^a | - | - | - |
| $E_{loc} (x^{e-2})$ | 1.62 ± 0.10 | 1.67 ± 0.10 | 1.68 ± 0.11 | 0.035 ^a | 0.027 | 0.044 | 0.432 |
| L_p | 84.64 ± 5.43 | 82.67 ± 6.18 | 81.55 ± 5.59 | 0.100 ^a | - | - | - |
| $C_p (x^{e-2})$ | 4.49 ± 0.39 | 4.51 ± 0.39 | 4.53 ± 0.38 | 0.958 ^a | - | - | - |
| γ | 7.23 ± 0.23 | 7.21 ± 0.24 | 7.19 ± 0.18 | 0.704 ^a | - | - | - |
| λ | 1.38 ± 0.02 | 1.38 ± 0.02 | 1.38 ± 0.01 | 0.581 ^a | - | - | - |
| σ | 5.23 ± 0.15 | 5.22 ± 0.15 | 5.21 ± 0.13 | 0.835 ^a | - | - | - |

Abbreviations: AUC = area under the curve; E_{glob} = the global efficiency; E_{loc} = the local efficiency; L_p = the shortest path length; C_p = the clustering coefficient; γ = the normalized clustering coefficient; λ = the normalized shortest path length; σ = the small-world index

IFGoperc, supplementary motor area (SMA), insula and left orbital superior frontal gyrus (ORBsup) and angular gyrus (Table 4; Fig. 3b). Notably, compared with controls, the CSVD-m group showed significantly decreased E_{nodal} only in the left angular gyrus, while the CSVD-s group showed significantly increased E_{nodal} in the pallidum.

Altered Network Efficiency Related to Cognitive Performance in CSVD Patients

For global/local efficiency and significantly altered nodal efficiencies among groups, participants Pearson's correlations with cognitive parameters were calculated. Intriguingly, we observed significant correlations ($p < 0.05$, FDR corrected [30]) between network efficiencies and all cognitive parameters for the CSVD-s group (Fig. 4a), and

the involved regions mainly included the bilateral caudate nucleus, right IFGoperc, SMA and left angular gyrus. Briefly, network efficiency in CSVD-s patients was significantly positively correlated with MoCA, AVLT and SDMT scores and negatively correlated with SCWT and TMT scores (Fig. 5). Moreover, only the left pallidum showed significant correlations with SDMT and TMT scores in the CSVD-m group (Fig. 4b).

Discussion

In this study, the topological organization of WM structural networks was investigated using probabilistic diffusion tractography and graph theory. Compared with CSVD-m patients and healthy controls, CSVD-s patients exhibited

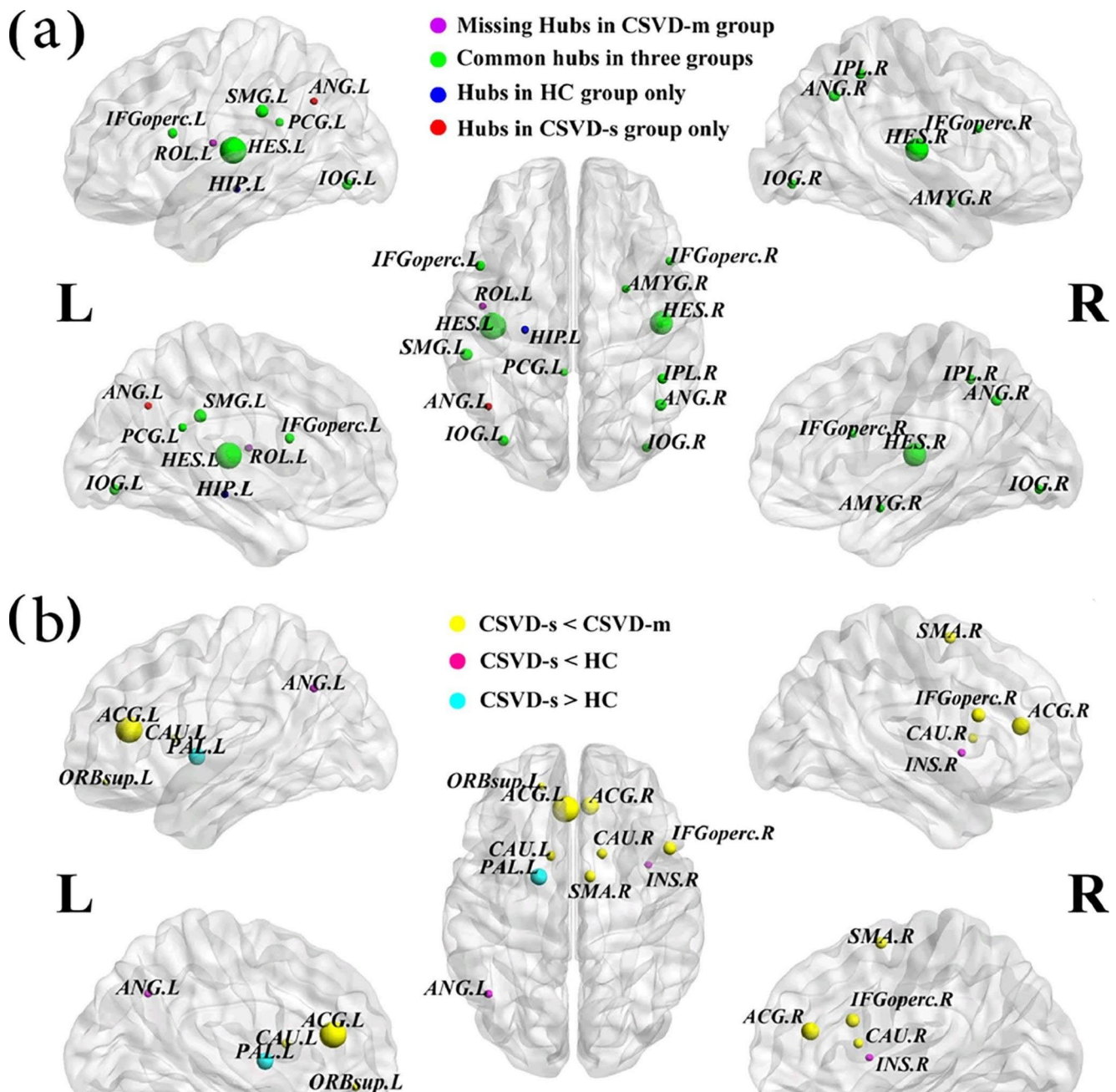


Fig. 3 Hub region distributions in the WM structural networks and nodes with altered efficiency among the three groups (a) Hub nodes are displayed with different node sizes indicating their nodal efficiency values. (b) The CSVD-s group exhibited significantly

significantly decreased E_{loc} , which implied a disturbance in information exchange in the structural brain network of CSVD-s patients. Moreover, widespread decreased E_{nodal} in CSVD-s patients was found mainly in the cognitive functional regions. Intriguingly, significant correlations between network efficiency and cognitive performance scores were detected mainly in CSVD-s patients. These findings revealed the disruption of topological organization in

increased nodal efficiency, and the scaled node sizes indicate the F values in the ANCOVA test. The brain graphs were visualized by using BrainNet Viewer software (<http://www.nitrc.org/projects/bnv/>). For the abbreviations of nodes, see Supplementary Table 1

structural networks in patients with CSVD, highlighted the importance of network analysis, and provided insights promoting a better understanding of the relationship between altered structural networks and cognitive deficits in patients with different CSVD burdens.

The human brain is understood to be a complex network with small-world properties, characterized by high local clustering and short path lengths, reflecting a balance

Table 3 Hub regions of WM networks in both the CSVD and control groups

| CSVD-s | CSVD-m | | HC | | |
|--------------|-----------------------------|------------|-----------------------------|--------------|-----------------------------|
| regions | $E_{\text{nodal}}(x^{e-2})$ | regions | $E_{\text{nodal}}(x^{e-2})$ | regions | $E_{\text{nodal}}(x^{e-2})$ |
| IFGoperc.L | 2.67 | IFGoperc.L | 2.86 | IFGoperc.L | 2.85 |
| IFGoperc.R | 2.48 | IFGoperc.R | 2.64 | IFGoperc.R | 2.73 |
| PCG.L | 2.44 | PCG.L | 2.52 | PCG.L | 2.56 |
| AMYG.R | 2.44 | AMYG.R | 2.52 | AMYG.R | 2.58 |
| IOG.L | 2.70 | IOG.L | 2.77 | IOG.L | 2.79 |
| IOG.R | 2.53 | IOG.R | 2.63 | IOG.R | 2.65 |
| IPL.R | 2.62 | IPL.R | 2.67 | IPL.R | 2.67 |
| SMG.L | 2.99 | SMG.L | 2.98 | SMG.L | 3.07 |
| ANG.R | 2.85 | ANG.R | 2.81 | ANG.R | 2.77 |
| HES.L | 4.73 | HES.L | 4.99 | HES.L | 5.07 |
| HES.R | 4.33 | HES.R | 4.48 | HES.R | 4.65 |
| <i>ROL.L</i> | 2.38 | | | <i>ROL.L</i> | 2.50 |
| <i>HIPL</i> | 2.41 | | | <i>ANG.L</i> | 2.53 |

Abbreviations: WM=white matter; E_{nodal} = nodal efficiency. E_{nodal} represents the AUC value of nodal efficiency across thresholds; For the abbreviations of regions, see Supplementary Table 1

between global integration and local segregation [31]. In this study, both CSVD patients and controls showed small-world properties of WM structural networks, which was consistent with previous studies of structural networks in CSVD patients [32], compared with the CSVD-m and control groups, the CSVD-s group exhibited significantly decreased E_{loc} , which means that the structural network has decreased efficiency in information processing and transfer in CSVD-s patients [33]. A considerable amount of research has shown that WM integrity is widely impaired in CSVD patients [34–36], and damage to WM leads to a breakdown in the structural and functional connections among specific brain regions [35, 37, 38], which cause reduced network efficiency [39]. Some researchers have suggested that disconnections between brain regions cause reduced network

efficiency [39]. E_{loc} quantifies the resistance of a network to small-scale damage. Therefore, a reduced E_{loc} means that when one region is damaged or disconnected, its connections with linked regions are dramatically affected [40]. Our previous study on the functional brain networks revealed significantly decreased E_{loc} in CSVD patients with CMBs [41]. In addition, compared with the CSVD-m group, the CSVD-s group had more severe pathological changes, more diverse MRI features and more severe topological disruption. Therefore, compared with the control group, only the CSVD-s group changed significantly, while no significant change was observed in the CSVD-m group.

Apart from studying the global properties, we also investigated the nodal topology of structural networks. Hub regions occupy a central position and interact with many brain regions in the network, supporting their diverse functional roles across a broad range of tasks and widespread dynamic coupling within and across networks [42]. However, due to the high level of centrality of hub regions, these regions are susceptible to disconnection and dysfunction in brain diseases [42]. We defined the hub regions of brain structural networks according to the nodal efficiency of the network and found that the three groups had highly similar hub distributions, with hub regions mainly in the frontal gyri (bilateral IFGoperc), occipital gyri (bilateral IOG), parietal (right inferior parietal gyrus, angular gyrus and left SMG), temporal gyri (bilateral Heschl gyrus and right amygdala) and left posterior cingulate gyrus, supporting the view that the key regions of the structural network can tolerate developmental alterations and disease [12]. In addition, the CSVD-s and control groups each had an additional hub region in the left hippocampus and angular gyrus, respectively, and the CSVD-m group lacked the left Rolandic operculum as a hub region. This may be due to the changes in the brain structural networks during the course of the

Table 4 Brain regions showing significantly altered nodal efficiency among the three groups for the WM networks

| Module | Region | $E_{\text{nodal}}(x^{e-2})$ | | | p value (ANCOVA) | p value (post-hoc) | | |
|---------------|------------|-----------------------------|-------------|-------------|------------------|--------------------|-------------------|---------------|
| | | CSVD-s | CSVD-m | HC | | CSVD-s vs. HC | CSVD-s vs. CSVD-m | CSVD-m vs. HC |
| attention | ORBsup.L | 1.64 ± 0.24 | 1.73 ± 0.25 | 1.67 ± 0.25 | 0.042 | N.S. | 0.007 | N.S. |
| attention | IFGoperc.R | 2.48 ± 0.27 | 2.64 ± 0.37 | 2.73 ± 0.29 | 0.015 | 0.002 | 0.042 | N.S. |
| attention | ANG.L | 2.37 ± 0.34 | 2.36 ± 0.37 | 2.53 ± 0.44 | 0.037 | 0.045 | N.S. | 0.012 |
| sensory/motor | SMA.R | 1.14 ± 0.23 | 1.26 ± 0.28 | 1.22 ± 0.27 | 0.021 | N.S. | 0.005 | N.S. |
| sensory/motor | INS.R | 1.84 ± 0.24 | 1.95 ± 0.32 | 2.02 ± 0.26 | 0.042 | 0.008 | N.S. | N.S. |
| DMN | ACG.L | 0.90 ± 0.13 | 0.97 ± 0.16 | 1.02 ± 0.19 | 0.002 | 0.001 | 0.015 | N.S. |
| DMN | ACG.R | 1.33 ± 0.22 | 1.44 ± 0.32 | 1.53 ± 0.33 | 0.007 | 0.006 | 0.041 | N.S. |
| Subcortical | CAU.L | 0.57 ± 0.16 | 0.68 ± 0.21 | 0.73 ± 0.22 | 0.030 | 0.022 | 0.027 | N.S. |
| Subcortical | CAU.R | 0.50 ± 0.09 | 0.58 ± 0.18 | 0.62 ± 0.16 | 0.027 | 0.003 | 0.035 | N.S. |
| Subcortical | PAL.L | 1.11 ± 0.79 | 0.88 ± 0.34 | 0.78 ± 0.26 | 0.008 | 0.007 | N.S. | N.S. |

Abbreviations: DMN= default mode network; N.S.= not significant. E_{nodal} represents the AUC values (mean ± SD) of the nodal efficiency of each group. For the abbreviations of regions, see Supplementary Table 1

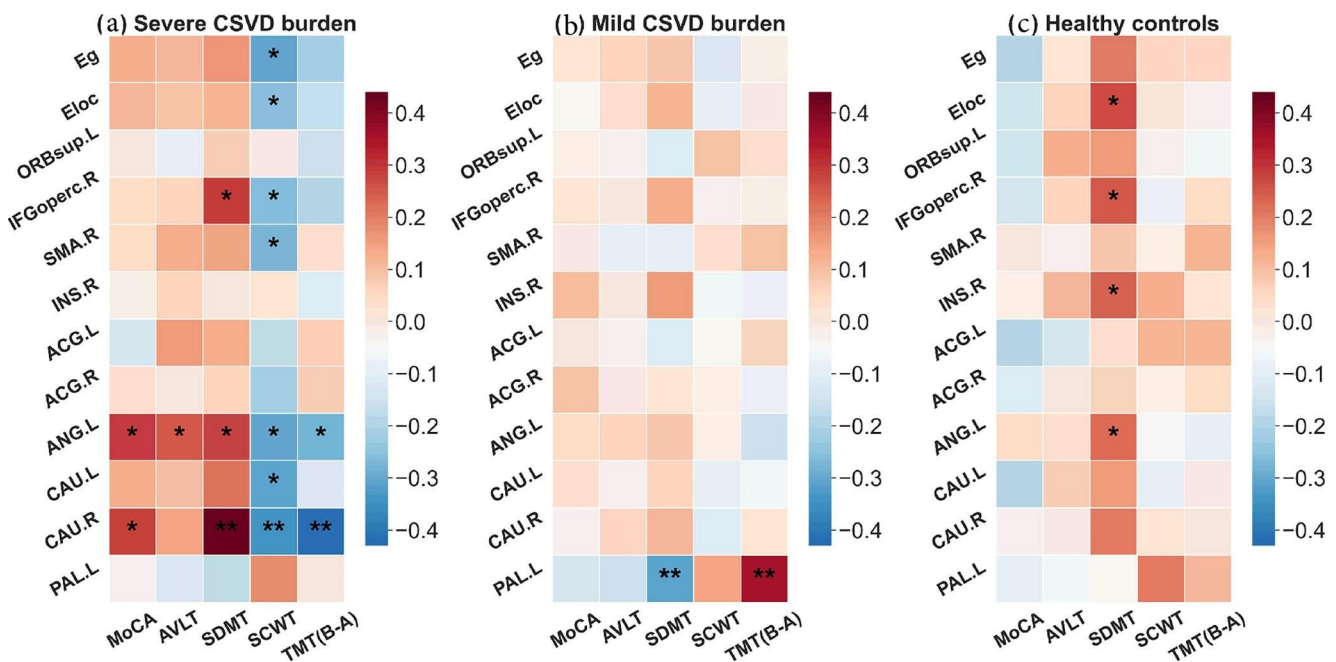


Fig. 4 Pearson's correlations between nodal efficiency and cognitive parameters in both the CSVD and control groups (a–c) Heat map of the correlation coefficient between nodal efficiency of disrupted regions and cognitive tests scores for the CSVD-s group, CSVD-m group and controls, respectively. *: $p < 0.05$, **: $p < 0.01$.

disease in CSVD patients, which affect the optimal paths of information transmission and ultimately lead to alterations in the hub distribution.

In this study, we also researched nodal efficiency and observed that the CSVD-s group had decreased E_{nodal} in nine brain regions, primarily located in subcortical, DMN, motor and attention functional modules [43], compared with the CSVD-m or control groups. Several studies have consistently shown that nodal efficiency decreased in brain regions associated with these functional modules in CSVD patients [16, 44, 45]. In addition, we found that the decrease in nodal efficiency was more severe in CSVD-s patients. Significantly decreased nodal efficiency in the CSVD-s group indicated that the ability to transmit information between this node and other nodes in the network decreased. With the progression of the disease, TNF- α expression in endothelial cells increases [46]. TNF- α increases blood brain barrier (BBB) permeability by inhibiting the expression of tight junction complexes [47]. Leakage of inflammatory substances into the brain through a disrupted BBB leads to central nervous system (CNS) inflammation [48]. In the presence of TNF- α , microglia can promote the release of glutamate from astrocytes, thereby enhancing the excitotoxicity of neurons [49]. In excitotoxicity, excessive release of glutamate leads to calcium overload in neurons, resulting in neuronal dysfunction, necrosis or apoptosis. Therefore, the destruction of the brain structure is more severe in CSVD-s

patients, and it is not difficult to understand that the E_{nodal} reduction is more significant in this group. Intriguingly, the CSVD-s group showed increased E_{nodal} in the pallidum. We hypothesize that this is a compensatory mechanism of the brain for regions with reduced E_{nodal} .

The CSVD burden is an important predictor for cognitive impairment in patients [50]. However, the role of brain structural network efficiency in the cognitive decline of CSVD patients has not yet been explored. We observed significant correlations between E_{nodal} and cognitive parameters in the CSVD-s group in the bilateral caudate nucleus, right IFGoperc, SMA and left angular gyrus. Importantly, E_{nodal} in the right caudate nucleus and left angular gyrus was significantly correlated with all five cognitive parameters. The caudate nucleus was suggested to be an important part of the brain's learning and memory system and plays a role in stereotyped and repetitive functions [51]. The angular gyrus and its connectivity with other brain regions are involved in memory function to different degrees [52]. Moreover, the IFGoperc, a brain region whose function encompasses both social cognition and emotion, serves as both a sensory-cognitive integration area and a control node of the ventral attention network [53]. Damage to the SMA region can affect executive function/cognitive control [54]. Through the mediation of E_{nodal} , these regions affect the cognitive function of the brain from multiple perspectives. We infer that the right caudate nucleus and left angular gyrus may

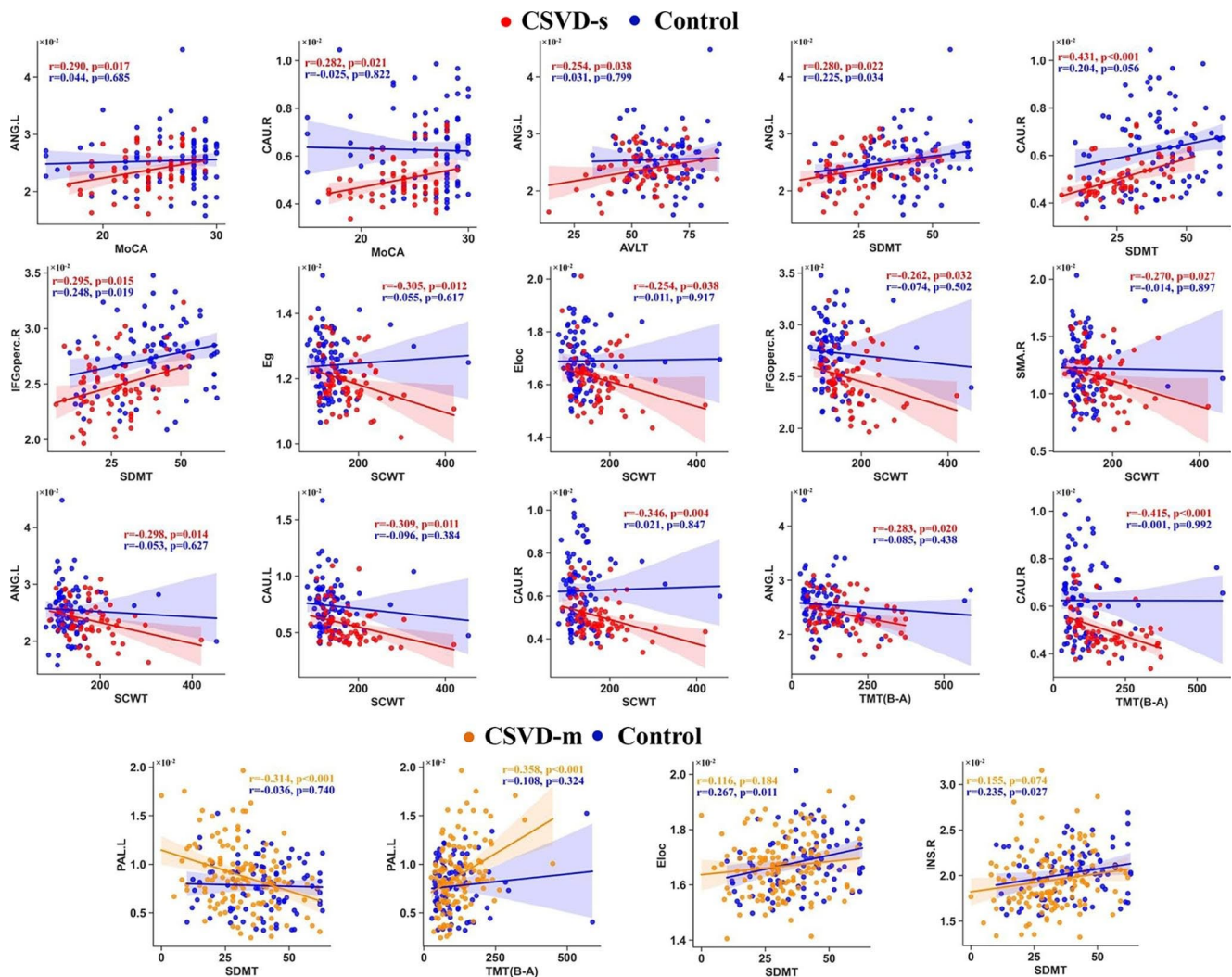


Fig. 5 Scatter plots showing the significant (all $p < 0.05$, FDR corrected) Pearson's correlations between network efficiency and cognitive parameters

The red, orange and blue represent the CSVD-s, CSVD-m and con-

trol groups respectively. Linear regression lines with 95% confidence intervals for the best-fit line (shading area), as well as r (partial correlation coefficient) and p values, are provided. For the abbreviations of nodes, see Supplementary Table 1

be two key areas that are more correlated with the severity of cognition, which is important for the exploration of neurophysiological mechanisms in CSVD-s patients. Moreover, all network efficiencies were significantly correlated with the SCWT scores, indicating that CSVD-s patients were most susceptible to impairment of visual search speed, working memory and conflict monitoring ability. Based on Pearson's correlation analysis, we speculate that only when the CSVD burden reaches a certain level will substantial damage to the brain structure occur, resulting in a linear decline in cognitive function. These results highlight the importance of investigating the correlation between network metrics and cognitive function in patients with different CSVD burdens, suggesting that early screening, diagnosis, detection and treatment of CSVD patients could prevent or delay cognitive decline.

Some limitations in this study should be considered. First, the use of a cross-sectional design implied that no conclusion about the temporality of alterations in CSVD burden, network properties, and cognition can be obtained. Second, this study only elaborated on disrupted WM structural networks, and follow-up studies should be conducted to combine structural and functional MR imaging to provide a comprehensive understanding with regard to the structure–function coupling relationship. Third, although the CSVD burden was introduced in our study to compensate for the shortcomings of a single neuroimaging feature, we still need to investigate whether different scoring features have significant differences in brain structural changes under the same burden score.

control groups respectively. Linear regression lines with 95% confidence intervals for the best-fit line (shading area), as well as r (partial correlation coefficient) and p values, are provided. For the abbreviations of nodes, see Supplementary Table 1

Conclusion

Using probabilistic diffusion tractography and graph theory, brain WM networks of CSVD are characterized by decreased local specialization, as well as widespread reduced network efficiency in cognitive functional regions. Patients with different CSVD burdens have segregated disruptions in WM network topology and associations with cognitive dysfunction. These findings expanded our understanding of brain structural alterations underlying CSVD and provided new theoretical bases for assessing the severity of CSVD.

Supplementary Information The online version contains supplementary material available at <https://doi.org/10.1007/s12035-023-03597-0>.

Author Contributions All authors contributed to the study conception and design. Conceptualization: Mengmeng Feng, Hongwei Wen, Changhu Liang, Lingfei Guo. Data curation: Mengmeng Feng, Haotian Xin, Chaofan Sui, Yian Gao. Formal analysis: Mengmeng Feng, Hongwei Wen, Shengpei Wang. Funding acquisition: Hongwei Wen, Lingfei Guo. Investigation: Mengmeng Feng, Hongwei Wen, Haotian Xin, Shengpei Wang, Chaofan Sui, Yian Gao. Methodology: Hongwei Wen, Shengpei Wang. Project administration: Changhu Liang, Lingfei Guo. Resources: Mengmeng Feng, Haotian Xin, Chaofan Sui, Yian Gao, Changhu Liang, Lingfei Guo. Software: Hongwei Wen, Shengpei Wang. Supervision: Changhu Liang, Lingfei Guo. Validation: Mengmeng Feng, Hongwei Wen, Haotian Xin, Shengpei Wang, Chaofan Sui, Yian Gao, Changhu Liang, Lingfei Guo. Visualization: Mengmeng Feng, Hongwei Wen. Writing-original draft: Mengmeng Feng, Hongwei Wen. Writing-review & editing: Mengmeng Feng, Hongwei Wen, Haotian Xin, Shengpei Wang, Chaofan Sui, Yian Gao, Changhu Liang, Lingfei Guo. All authors read and approved the final manuscript.

Funding This work was supported by grants from the National Natural Science Foundation of China (grant number 32100902,82272072), the Fundamental Research Funds for the Central Universities (grant number SWU118065), the Natural Science Foundation of Shandong Province (grant number ZR2020MH288), the Technology Development Plan of Jinan (grant number 201907052), Medical and Health Science and Technology Development Project of Shandong Province (grant number 2016WS0529) and Funding for Study Abroad Program by Shandong Province (grant number 201803059).

Data Availability The datasets generated during and analysed during the current study are not publicly available due to [REASON(S) WHY DATA ARE NOT PUBLIC] but are available from the corresponding author on reasonable request.

Declarations

Competing Interests The authors have no relevant financial or non-financial interests to disclose.

Ethics Approval This study was performed in line with the principles of the Declaration of Helsinki. Approval was granted by the Ethics Committee of Shandong Provincial Hospital Affiliated to Shandong First Medical university.

Consent to Participate Informed consent was obtained from all individual participants included in the study.

Consent to Publish The authors affirm that human research participants provided informed consent for publication of the images in Figures.

Open Access This article is licensed under a Creative Commons Attribution 4.0 International License, which permits use, sharing, adaptation, distribution and reproduction in any medium or format, as long as you give appropriate credit to the original author(s) and the source, provide a link to the Creative Commons licence, and indicate if changes were made. The images or other third party material in this article are included in the article's Creative Commons licence, unless indicated otherwise in a credit line to the material. If material is not included in the article's Creative Commons licence and your intended use is not permitted by statutory regulation or exceeds the permitted use, you will need to obtain permission directly from the copyright holder. To view a copy of this licence, visit <http://creativecommons.org/licenses/by/4.0/>.

References

1. Cannistraro RJ, Badi M, Eidelman BH, Dickson DW, Middlebrooks EH, Meschia JF (2019) CNS small vessel disease: a clinical review. *Neurology* 92:1146–1156. <https://doi.org/10.1212/wnl.0000000000007654>
2. Wardlaw JM, Smith C, Dichgans M (2019) Small vessel disease: mechanisms and clinical implications. *Lancet Neurol* 18:684–696. [https://doi.org/10.1016/s1474-4422\(19\)30079-1](https://doi.org/10.1016/s1474-4422(19)30079-1)
3. Duering M, Biessels GJ, Brodtmann A, Chen C, Cordonnier C, de Leeuw FE, Debette S et al (2023) Neuroimaging standards for research into small vessel disease—advances since 2013. *Lancet Neurol* 22:602–618. [https://doi.org/10.1016/s1474-4422\(23\)00131-x](https://doi.org/10.1016/s1474-4422(23)00131-x)
4. Klarenbeek P, van Oostenbrugge RJ, Rouhl RP, Knottnerus IL, Staals J (2013) Ambulatory blood pressure in patients with lacunar stroke: association with total MRI burden of cerebral small vessel disease. *Stroke* 44:2995–2999. <https://doi.org/10.1161/strokeaha.113.002545>
5. Pasi M, Sugita L, Xiong L, Charidimou A, Boulouis G, Pongitakmetha T, Singh S et al (2021) Association of Cerebral Small Vessel Disease and Cognitive decline after Intracerebral Hemorrhage. *Neurology* 96:e182–e192. <https://doi.org/10.1212/wnl.0000000000011050>
6. Banerjee G, Jang H, Kim HJ, Kim ST, Kim JS, Lee JH, Im K et al (2018) Total MRI small Vessel Disease Burden correlates with cognitive performance, cortical atrophy, and Network Measures in a memory Clinic Population. *J Alzheimers Dis* 63:1485–1497. <https://doi.org/10.3233/jad-170943>
7. Gu Y, Zhao P, Feng W, Xia X, Tian X, Yan Y, Wang X et al (2022) Structural brain network measures in elderly patients with cerebral small vessel disease and depressive symptoms. *BMC Geriatr* 22:568. <https://doi.org/10.1186/s12877-022-03245-7>
8. Hatate J, Miwa K, Matsumoto M, Sasaki T, Yagita Y, Sakaguchi M, Kitagawa K et al (2016) Association between cerebral small vessel diseases and mild parkinsonian signs in the elderly with vascular risk factors. *Parkinsonism Relat Disord* 26:29–34. <https://doi.org/10.1016/j.parkreldis.2016.02.011>
9. Chen H, Wan H, Zhang M, Liu G, Wang X, Wang Z, Ma H et al (2021) Cerebral small vessel disease may worsen motor function, cognition, and mood in Parkinson's disease. *Parkinsonism Relat Disord* 83:86–92. <https://doi.org/10.1016/j.parkreldis.2020.12.025>
10. Zhang Y, Zhang Z, Zhang M, Cao Y, Yun W (2021) Correlation between retinal microvascular abnormalities and total magnetic resonance imaging Burden of Cerebral Small Vessel Disease in

- patients with type 2 diabetes. *Front Neurosci* 15:727998. <https://doi.org/10.3389/fnins.2021.727998>
11. Behrens TE, Johansen-Berg H, Woolrich MW, Smith SM, Wheeler-Kingshott CA, Boulby PA, Barker GJ et al (2003) Non-invasive mapping of connections between human thalamus and cortex using diffusion imaging. *Nat Neurosci* 6:750–757. <https://doi.org/10.1038/nn1075>
 12. Wen H, Liu Y, Rekik I, Wang S, Zhang J, Zhang Y, Peng Y et al (2017) Disrupted topological organization of structural networks revealed by probabilistic diffusion tractography in Tourette syndrome children. *Hum Brain Mapp* 38:3988–4008. <https://doi.org/10.1002/hbm.23643>
 13. Xu M, Tan X, Zhang X, Guo Y, Mei Y, Feng Q, Xu Y et al (2017) Alterations of white matter structural networks in patients with non-neuropsychiatric systemic lupus erythematosus identified by probabilistic tractography and connectivity-based analyses. *Neuroimage Clin* 13:349–360. <https://doi.org/10.1016/j.nicl.2016.12.021>
 14. Bullmore E, Sporns O (2009) Complex brain networks: graph theoretical analysis of structural and functional systems. *Nat Rev Neurosci* 10:186–198. <https://doi.org/10.1038/nrn2575>
 15. Drakesmith M, Caeyenberghs K, Dutt A, Zammit S, Evans CJ, Reichenberg A, Lewis G et al (2015) Schizophrenia-like topological changes in the structural connectome of individuals with sub-clinical psychotic experiences. *Hum Brain Mapp* 36:2629–2643. <https://doi.org/10.1002/hbm.22796>
 16. Xu X, Lau KK, Wong YK, Mak HKF, Hui ES (2018) The effect of the total small vessel disease burden on the structural brain network. *Sci Rep* 8:7442. <https://doi.org/10.1038/s41598-018-25917-4>
 17. Frey BM, Petersen M, Schlemm E, Mayer C, Hanning U, Engelke K, Fiehler J et al (2021) White matter integrity and structural brain network topology in cerebral small vessel disease: the Hamburg city health study. *Hum Brain Mapp* 42:1406–1415. <https://doi.org/10.1002/hbm.25301>
 18. Heinen R, Vlegels N, de Bresser J, Leemans A, Biessels GJ, Reijmer YD (2018) The cumulative effect of small vessel disease lesions is reflected in structural brain networks of memory clinic patients. *Neuroimage Clin* 19:963–969. <https://doi.org/10.1016/j.nicl.2018.06.025>
 19. Bergeron D, Flynn K, Verret L, Poulin S, Bouchard RW, Bocti C, Fülöp T et al (2017) Multicenter Validation of an MMSE-MoCA Conversion table. *J Am Geriatr Soc* 65:1067–1072. <https://doi.org/10.1111/jgs.14779>
 20. Lu J, Li D, Li F, Zhou A, Wang F, Zuo X, Jia X-F et al (2011) Montreal cognitive assessment in detecting cognitive impairment in chinese elderly individuals: a population-based study. *J Geriatr Psychiatr Neurol* 24:184–190. <https://doi.org/10.1177/0891988711422528>
 21. Putcha D, Brickhouse M, Wolk DA, Dickerson BC, Alzheimers Dis Neuroimaging I (2019) Fractionating the Rey Auditory Verbal Learning Test: distinct roles of large-scale cortical networks in prodromal Alzheimer's disease. *Neuropsychologia* 129:83–92. <https://doi.org/10.1016/j.neuropsychologia.2019.03.015>
 22. Benedict RH, DeLuca J, Phillips G, LaRocca N, Hudson LD, Rudick R (2017) Validity of the Symbol Digit Modalities Test as a cognition performance outcome measure for multiple sclerosis. *Mult Scler* 23:721–733. <https://doi.org/10.1177/1352458517690821>
 23. Wei M, Shi J, Li T, Ni J, Zhang X, Li Y, Kang S et al (2018) Diagnostic accuracy of the Chinese Version of the trail-making test for Screening Cognitive Impairment. *J Am Geriatr Soc* 66:92–99. <https://doi.org/10.1111/jgs.15135>
 24. Scarpina F, Tagini S (2017) The Stroop Color and Word Test. *Front Psychol* 8:557. <https://doi.org/10.3389/fpsyg.2017.00557>
 25. Behrens TEJ, Johansen H, Berg S, Jbabdi et al (2007) Probabilistic diffusion tractography with multiple fibre orientations: What can we gain? *NeuroImage* 34:144–155
 26. Tzourio-Mazoyer N, Landeau B, Papathanassiou D, Crivello F, Etard O, Delcroix N, Mazoyer B et al (2002) Automated anatomical labeling of activations in SPM using a macroscopic anatomical parcellation of the MNI MRI single-subject brain. *NeuroImage* 15:273–289. <https://doi.org/10.1006/nimg.2001.0978>
 27. Cao Q, Shu N, An L, Wang P, Sun L, Xia MR, Wang JH et al (2013) Probabilistic diffusion tractography and graph theory analysis reveal abnormal white matter structural connectivity networks in drug-naive boys with attention deficit/hyperactivity disorder. *J Neurosci* 33:10676–10687. <https://doi.org/10.1523/jneurosci.4793-12.2013>
 28. Latora V, Marchiori M (2001) Efficient behavior of small-world networks. *Phys Rev Lett* 87:198701
 29. Wang J, Wang X, Xia M, Liao X, Evans A, He Y (2015) GRETNA: a graph theoretical network analysis toolbox for imaging connectomics. *Front Hum Neurosci* 9:386. <https://doi.org/10.3389/fnhum.2015.00386>
 30. Benjamini Y, Hochberg Y (1995) Controlling the false Discovery rate: a practical and powerful Approach to multiple testing. *J Royal Stat Soc Ser B: Methodological* 57:289–300
 31. Sporns O (2011) The human connectome: a complex network. *Ann N Y Acad Sci* 1224:109–125. <https://doi.org/10.1111/j.1749-6632.2010.05888.x>
 32. Hagmann P, Cammoun L, Gigandet X, Meuli R, Honey CJ, Wedeen VJ, Sporns O (2008) Mapping the structural core of human cerebral cortex. *PLoS Biol* 6:e159. <https://doi.org/10.1371/journal.pbio.0060159>
 33. Sporns O, Honey CJ (2006) Small worlds inside big brains. *Proc Natl Acad Sci U S A* 103:19219–19220. <https://doi.org/10.1073/pnas.0609523103>
 34. Pappa JM, de Groot M, de Koning I, Mattace-Raso FU, van der Lugt A, Vernooij MW, Niessen WJ et al (2014) Cerebral small vessel disease affects white matter microstructure in mild cognitive impairment. *Hum Brain Mapp* 35:2836–2851. <https://doi.org/10.1002/hbm.22370>
 35. Liu C, Zou L, Tang X, Zhu W, Zhang G, Qin Y, Zhu W (2020) Changes of white matter integrity and structural network connectivity in nondemented cerebral small-vessel disease. *J Magn Reson Imaging* 51:1162–1169. <https://doi.org/10.1002/jmri.26906>
 36. van der Holst HM, Tuladhar AM, Zerbi V, van Uden IWM, de Laat KF, van Leijssen EMC, Ghafoorian M et al (2018) White matter changes and gait decline in cerebral small vessel disease. *Neuroimage Clin* 17:731–738. <https://doi.org/10.1016/j.nicl.2017.12.007>
 37. Tuladhar AM, Lawrence A, Norris DG, Barrick TR, Markus HS, de Leeuw FE (2017) Disruption of rich club organisation in cerebral small vessel disease. *Hum Brain Mapp* 38:1751–1766. <https://doi.org/10.1002/hbm.23479>
 38. Tuladhar AM, van Dijk E, Zwiers MP, van Norden AG, de Laat KF, Shumskaya E, Norris DG et al (2016) Structural network connectivity and cognition in cerebral small vessel disease. *Hum Brain Mapp* 37:300–310. <https://doi.org/10.1002/hbm.23032>
 39. Zhu Y, Lu T, Xie C, Wang Q, Wang Y, Cao X, Su Y et al (2020) Functional disorganization of small-world brain networks in patients with ischemic leukoariosis. *Front Aging Neurosci* 12:203. <https://doi.org/10.3389/fnagi.2020.00203>
 40. Suo X, Lei D, Chen F, Wu M, Li L, Sun L, Wei X et al (2017) Anatomical insights into disrupted small-world networks in Pediatric Posttraumatic stress disorder. *Radiology* 282:826–834. <https://doi.org/10.1148/radiol.2016160907>
 41. Xin H, Wen H, Feng M, Gao Y, Sui C, Zhang N, Liang C et al (2022) Disrupted topological organization of resting-state

- functional brain networks in cerebral small vessel disease. *Hum Brain Mapp.* <https://doi.org/10.1002/hbm.25808>
42. van den Heuvel MP, Sporns O (2013) Network hubs in the human brain. *Trends Cogn Sci* 17:683–696. <https://doi.org/10.1016/j.tics.2013.09.012>
 43. Yong H, Jinhui W, Liang W, Chen ZJ, Chaogan Y, Hong Y, Hehan T et al (2009) Uncovering intrinsic Modular Organization of spontaneous brain activity in humans. *PLoS ONE* 4:e5226
 44. Wang Y, Liu X, Hu Y, Yu Z, Wu T, Wang J, Liu J et al (2022) Impaired functional network properties contribute to white matter hyperintensity related cognitive decline in patients with cerebral small vessel disease. *BMC Med Imaging* 22:40. <https://doi.org/10.1186/s12880-022-00769-7>
 45. Xie X, Shi Y, Zhang J (2017) Structural network connectivity impairment and depressive symptoms in cerebral small vessel disease. *J Affect Disord* 220:8–14. <https://doi.org/10.1016/j.jad.2017.05.039>
 46. Elahy M, Jackaman C, Mamo JC, Lam V, Dhaliwal SS, Giles C, Nelson D et al (2015) Blood-brain barrier dysfunction developed during normal aging is associated with inflammation and loss of tight junctions but not with leukocyte recruitment. *Immun Ageing* 12:2. <https://doi.org/10.1186/s12979-015-0029-9>
 47. Trickler WJ, Mayhan WG, Miller DW (2005) Brain microvessel endothelial cell responses to tumor necrosis factor-alpha involve a nuclear factor kappa B (NF-kappaB) signal transduction pathway. *Brain Res* 1048:24–31. <https://doi.org/10.1016/j.brainres.2005.04.028>
 48. Wardlaw JM, Smith C, Dichgans M (2013) Mechanisms of sporadic cerebral small vessel disease: insights from neuroimaging. *Lancet Neurol* 12:483–497. [https://doi.org/10.1016/s1474-4422\(13\)70060-7](https://doi.org/10.1016/s1474-4422(13)70060-7)
 49. Linnerbauer M, Wheeler MA, Quintana FJ (2020) Astrocyte crosstalk in CNS inflammation. *Neuron* 108:608–622. <https://doi.org/10.1016/j.neuron.2020.08.012>
 50. Chen X, Wang J, Shan Y, Cai W, Liu S, Hu M, Liao S et al (2019) Cerebral small vessel disease: neuroimaging markers and clinical implication. *J Neurol* 266:2347–2362. <https://doi.org/10.1007/s00415-018-9077-3>
 51. Çırak M, Yağmurlu K, Kearns KN, Ribas EC, Urgan K, Shaffrey ME, Kalani MYS (2020) The Caudate Nucleus: its connections, Surgical Implications, and related complications. *World Neurosurg* 139:e428–e438. <https://doi.org/10.1016/j.wneu.2020.04.027>
 52. Sestieri C, Shulman GL, Corbetta M (2017) The contribution of the human posterior parietal cortex to episodic memory. *Nat Rev Neurosci* 18:183–192. <https://doi.org/10.1038/nrn.2017.6>
 53. Adolfi F, Couto B, Richter F, Decety J, Lopez J, Sigman M, Manes F et al (2017) Convergence of interoception, emotion, and social cognition: a twofold fMRI meta-analysis and lesion approach. *Cortex* 88:124–142. <https://doi.org/10.1016/j.cortex.2016.12.019>
 54. Sjöberg RL, Stålnacke M, Andersson M, Eriksson J (2019) The supplementary motor area syndrome and cognitive control. *Neuropsychologia* 129:141–145. <https://doi.org/10.1016/j.neuropsychologia.2019.03.013>

Publisher's Note Springer Nature remains neutral with regard to jurisdictional claims in published maps and institutional affiliations.